Euro. Jnl of Applied Mathematics (2019), *vol.* 30, *pp.* 196–218. © Cambridge University Press 2018
doi:10.1017/S0956792518000013

Pattern formation in bacterial colonies with density-dependent diffusion

JULIEN SMITH-ROBERGE, DAVID IRON
and THEODORE KOLOKOLNIKOV

Dalhousie University, Dept. Math&Stats, PO BOX 15000, Halifax, NS, Canada
emails: jsmirob@gmail.com, tkolokol@gmail.com, iron@mathstat.dal.ca

(*Received 9 May 2017; revised 8 January 2018; accepted 9 January 2018; first published online 28 January 2018*)

Recent experiments have shown that patterns can emerge in bacterial colonies genetically modified to have a drop in diffusion when population densities (detected via a quorum sensing mechanism) are sufficiently large. We examine one PDE model of this system, and construct its non-constant stationary solutions in the form of an interface for the bacterial density. We derive the equations for the interface motion and demonstrate analytically that such interface solution is stable when the diffusion rate of bacteria is large and the diffusion rate of signalling molecules, D_h, is small. We further demonstrate that increasing D_h induces a Hopf bifurcation, resulting in a loss of stability, which can lead to either complex spatio-temporal dynamics or extinction of pattern altogether. These results are confirmed by numerical simulations.

Key words: Bacterial aggregation, pattern formation, state-dependent diffusion

1 Introduction

Several species of bacteria move via a run and tumble mechanism—motion in a straight line (runs) punctuated by periods of random reorientation (tumbles)—which, for sufficiently large populations, can be modelled as diffusion. Moreover, by changing the ratio of runs to tumbles, a population can effectively change its diffusion rate. Such a change can give rise to chemotaxis and other types of non-linear diffusion, each of which may lead to the formation of patterns or other group behaviour [1]. Explaining such phenomena naturally leads to the development of mathematical models. Perhaps the best known of these is the Keller–Segel model [2], though the literature is replete with examples of reaction–diffusion type models where simple diffusion has been replaced by some non-linear variant [3–11].

The bacterial species *Vibrio fischeri* secretes acyl-homoserine lactone (AHL), a signalling molecule that acts as part of a quorum sensing mechanism [12]. When large populations of *V. fischeri* gather in one place, the concentration of AHL can reach sufficiently high levels to trigger changes in the behaviour of the bacteria. In the wild, this particular mechanism allows the bacteria to regulate bioluminescence. Similar quorum sensing mechanisms abound in nature [12]. Using techniques from synthetic biology, Liu *et al.* [13] introduced this mechanism to a strain of *Escherichia coli*, and coupled it to a pathway which controls run-and-tumble motility. The net effect is for the bacteria to have a sudden drop in

https://doi.org/10.1017/S0956792518000013 Published online by Cambridge University Press

diffusion when population density is large enough for the AHL concentration to surpass a given threshold. Similar population-dependent changes in diffusion are known to generate patterns [14–16]. Further experiments showed that these modified bacteria form patterns when grown on agar plates. The group proposed two partial differential equation (PDE) models to help explain this behaviour [13, 17].

The model introduced in [13, 17] is a one-dimensional non-linear PDE system:

$$p_t = (s(h)p)_{xx} + \gamma p\left(1 - \frac{p}{p_s}\right), \tag{1.1}$$

$$h_t = D_h h_{xx} + \alpha p - \beta h\ . \tag{1.2}$$

The quantities $p(x,t)$ and $h(x,t)$ denote the density of bacteria and AHL, respectively. AHL is produced by the bacteria at a rate α, and decays at a rate β. The constants γ and p_s represent, respectively, the logistic growth rate and equilibrium population of the bacteria. The diffusion rate D_h for h is assumed to be constant, whereas the diffusion rate of p is state-dependent on h. At low h concentration, bacteria diffuse freely. High h concentrations, however, trigger the synthetic genetic circuit described above, inducing a drop in the diffusion rate of the bacteria.

The drop in diffusion happens at some critical AHL concentration, h_c. This is modelled using a step function

$$s(h) = \begin{cases} D_- & h \leqslant h_c \\ D_+ & h > h_c \end{cases}, \qquad D_- > D_+\ . \tag{1.3}$$

More generally, the state-dependent diffusion is assumed to be a smoothed-out step function such as e.g.,

$$s(h) = (D_+ - D_-)\,\frac{1}{2}\left[\tanh\left(\frac{h - h_c}{\delta}\right) - 1\right] + D_+, \quad \delta \ll 1, \tag{1.4}$$

with a transition around $h = h_c$. See Appendix, for the derivation of the form of space-dependent diffusion from first principles.

We non-dimensionalize the system by rescaling $p = p_s\hat{p}$, $h = (\alpha p_s/\beta)\hat{h}$, $t = (1/\beta)\hat{t}$. Define rescaled parameters as $\hat{D}_h = D_h/\beta$, $\hat{D}_\pm = D_\pm/\gamma$, $\tau = \frac{\beta}{\gamma}$, $h_c = (\alpha p_s/\beta)\hat{h}_c$, $\delta = (\alpha p_s/\beta)\hat{\delta}$. After dropping the hats, we obtain the non-dimensionalized system:

$$\tau p_t = (s(h)p)_{xx} + p\,(1 - p)\,, \tag{1.5a}$$

$$h_t = D_h h_{xx} + p - h. \tag{1.5b}$$

These equations are solved on a finite domain, which, by choosing the correct scaling, we may take to be the unit interval, $[0, 1]$. We impose no-flux boundary conditions for both p and h.

In this paper, we explore non-linear patterns that occur for the model (1.5). Examples of such patterns are shown in Figures 1 and 7. To obtain analytical results, we concentrate on the limit of sharp step-like diffusion ($\delta \to 0$ in (1.4)), although we expect that our results are also valid for non-zero δ. In particular, we validate our asymptotic results using full numerics with non-zero but small δ.

https://doi.org/10.1017/S0956792518000013 Published online by Cambridge University Press

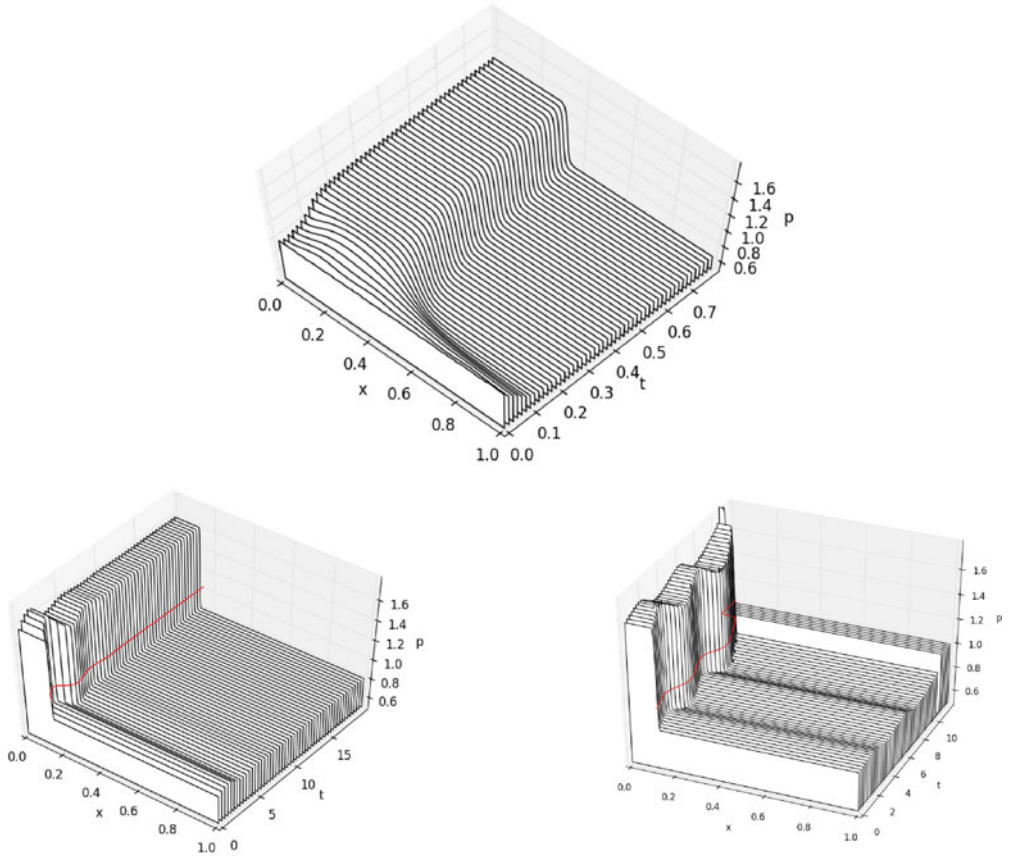


FIGURE 1. Top: Turing instability of a constant state resulting in a moving-interface pattern. The interface develops fully around $t \approx 0.15$, and eventually settles to a stationary state. ($D_h = 0.1$). Left: Evolution of the interface in the stable regime ($D_h = 0.19$). The red line tracks the motion of the interface. Right: Evolution of the interface in the unstable regime ($D_h = 0.202$). The red line tracks the motion of the interface. The interface is eventually destroyed. In each of the above simulations $\tau = 0$, and $s(h)$ is as given in (1.4) with $D_+ = 50$, $D_- = 100$, and with $\delta = 0.01$ in the top, $\delta = 0.001$ in the right and left.

In the limit of sharp step-like diffusion ($\delta \to 0$ in (1.4)), Turing analysis reveals that the constant state $h = p = 1$ of (1.5) is unstable (and therefore patterns form) provided that the transition point h_c occurs precisely at the steady state:

$$h_c = 1. \tag{1.5c}$$

More generally, Turing instability occurs when the drop in diffusion is sufficiently sharp at the steady state; namely, $D_h + s(1) < -s'(1)$. In the limit of sharp interface (1.4) with $\delta \to 0$, this condition is satisfied if and only if (1.5c) holds. Otherwise, the constant state is stable since it does not 'feel' the drop in diffusion, and no patterns are formed. Although in general, non-constant solutions are possible even when the constant states are Turing-stable (i.e., it is possible for constant and non-constant solutions to 'co-exist'),

https://doi.org/10.1017/S0956792518000013 Published online by Cambridge University Press

numerics of (1.5) suggest that in the limit of small δ, non-constant solutions are most robust precisely when (1.5c) holds.

Turing instability initiates pattern formation. As illustrated in Figure 1, the resulting pattern consists of (one or more) interfaces. Once formed, the interfaces start to move. Depending on the choice of parameters, the interface may eventually settle to a specific location, or it can undergo some rather complex dynamics (e.g., see Figure 1 bottom right, Figures 6 and 7). The main goal of this paper is to describe such interface solutions explicitly. In the limit of sharp diffusion drop, these solutions contain jump discontinuities. In Section 2, we derive an equation of a slow motion for a single discontinuity in the case where the diffusion of signalling molecules, D_h, is small. The resulting equation (see Proposition 1) is

$$x_0'(t) \sim \sqrt{D_h}\frac{\left(D_+/D_-\right)\left(1-x_0(t)\right)-x_0(t)}{\sqrt{\left(D_+/D_-\right)x_0(t)(1-x_0(t))}}. \tag{1.6}$$

This equation shows that $x_0(t) \to \frac{1}{D_-/D_+ +1}$ for large t. As such, the interface profile is stable when bacterial diffusion is large[1]. We then address the question of stability more generally, when D_h is not necessary small. In section 3, we use linear stability analysis to formulate the associated eigenvalue problem, and derive a transcendental equation that has the eigenvalues as its roots. Solving this equation numerically, we show that the system exhibits a Hopf bifurcation (see Figure 1). We conclude by showing that the linear stability analysis reproduces the eigenvalue derived via the equation of motion.

1.1 Turing instability

A preliminary insight is obtained by performing Turing analysis. The system (1.5) admits a trivial steady-state solution ($p = h = 1$). Take perturbations of the form

$$p = 1 + e^{\lambda t}e^{imx}\phi, \quad h = 1 + e^{\lambda t}e^{imx}\psi, \quad \phi, \psi \ll 1$$

which yields

$$\lambda\begin{pmatrix}\phi\\ \psi\end{pmatrix} = \begin{pmatrix}-\frac{m^2 s(1)+1}{\tau} & -\frac{m^2 s\prime(1)}{\tau}\\ 1 & -D_h m^2 - 1\end{pmatrix}\begin{pmatrix}\phi\\ \psi\end{pmatrix}.$$

Note that the trace of this matrix is $-\frac{m^2 s(1)+1}{\tau} - D_h m^2 - 1$, which is always negative. Therefore, the homogeneous state is unstable if and only if the determinant is negative, that is,

$$s(1)D_h m^4 + (D_h + s(1) + s'(1))m^2 + 1 < 0 \text{ for some } m > 0. \tag{1.7}$$

The determinant is positive for large m. Therefore, the instability of spatially uniform state occurs when $D_h + s(1) + s'(1) < 0$ as well as to having a positive descriminant, $(D_h + s(1) + s'(1))^2 - s(1)D_h > 0$.

[1] The slow motion is due to existence of a small eigenvalue and convergence of the ODE (1.6) to its steady state is equivalent to that eigenvalue being stable. One may ask about $O(1)$ eigenvalues. Numerical computations show that such eigenvalues do not exist for a single interface solution.

https://doi.org/10.1017/S0956792518000013 Published online by Cambridge University Press

In the case, where $s(h)$ is a near-step function with a sharp drop at $h = h_c$ such as in (1.4), the instability of a constant state will happen if and only if $h_c \sim 1$, that is, the drop in diffusion occurs precisely at the steady state $h = 1$.

There is some debate about what is the appropriate model for density-dependent diffusion: whether it should be $(sp)_{xx}$, $(sp_x)_x$, or some linear combination of both [13]. We include Appendix in which we argue, from first principles, that the former form is the appropriate way to model the diffusion. In fact, it is easy to see that the latter form *does not* have Turing instability: if we were to replace $(sp)_{xx}$ by $(sp_x)_x$ then the equation for ϕ becomes fully decoupled from ψ: $\lambda\tau\phi = -(s(1)m^2 + 1)\phi$, and as a result, λ is always negative.

Movivated by Turing analysis, in what follows we will assume $h_c = 1$, so that the constant state is Turing-unstable. Note that in [17] numerical simulations of (1.5) resulted only in transient pattern formation. The eventual steady state was homogeneous in space. This was due to a parameter choice which did not satisfy (1.7).

2 Interface motion

As with many non-linear PDE, general solutions are beyond our grasp. We begin with a selection of solutions for special cases. Our analysis will focus primarily on stationary and near-stationary solutions, and, beyond what has already been said about Turing instability, we will largely ignore the details behind a solution's transition from a nearly constant profile to one with large-scale spatial variations.

2.1 Jump conditions

We start by looking for stationary non-homogeneous solutions to equations (1.5) where we take $h_c = 1$,

$$s(h) = \begin{cases} D_- & h \leqslant 1 \\ D_+ & h > 1 \end{cases}, \quad D_- > D_+ \,. \tag{2.1}$$

We will construct a solution consisting of a single interface at $x = x_0$ as shown in Figure 2. First, let us suppose that $\tau p_t = 0$, that is either $\tau = 0$ or the interface is stationary. At the interface, we have $h = 1$, whereas p has a jump discontinuity. Outside the interface, p solves Fisher's equation $D_\pm p_{xx} = -p(1-p)$ for $x \neq x_0$ subject to jump conditions that we now derive.

Assume that $s(h) = D_-$ to the right of x_0, and $s(h) = D_+$ to the left; in other words $h(x)$ is decreasing as shown in Figure 2. Integrating (1.5a) in a small neighbourhood around x_0, we obtain

$$\begin{aligned} 0 &= \int_{x_0^-}^{x_0^+} (s(h)p)_{xx}dx + \int_{x_0^-}^{x_0^+} p(1-p)dx \qquad (\to 0) \\ &= D_- p_x(x_0^+, t) - D_+ p_x(x_0^-, t) \,. \end{aligned} \tag{2.2}$$

https://doi.org/10.1017/S0956792518000013 Published online by Cambridge University Press

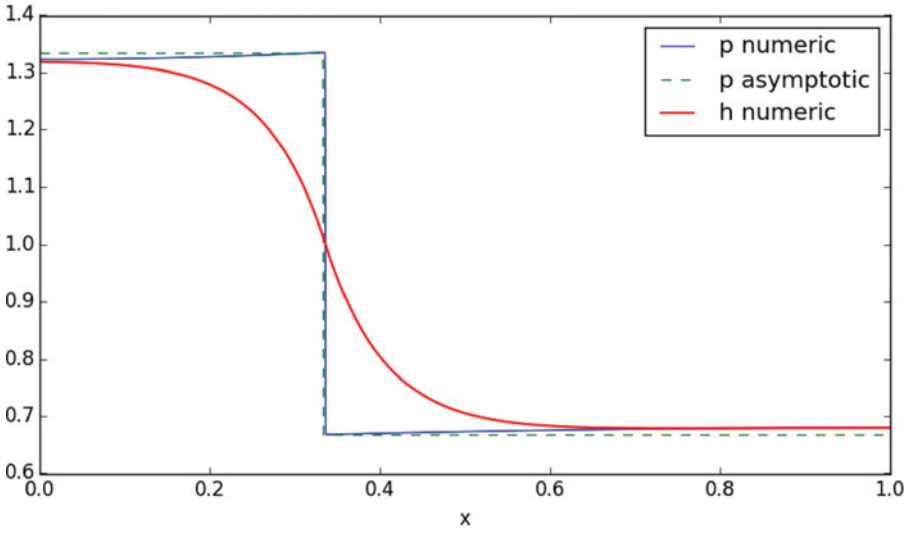


FIGURE 2. Numerically calculated solutions versus the piecewise constant approximation. Parameters are $D_h = 0.005$, $\tau = 0$, and with $s(h)$ as given in (1.4) with $D_+ = 50$, $D_- = 100$, $\delta = 0.001$.

Similarly, premultiplying (1.5*a*) by x before integrating yields

$$0 = D_- p(x_0^+, t) - D_+ p(x_0^-, t) \, . \tag{2.3}$$

From this, we see that p will have a discontinuity at x_0 (see Figure 2). The same calculation can be done for equation (1.5*b*) to obtain the following conditions:

$$0 = h_x(x_0^+, t) - h_x(x_0^-, t) \, , \tag{2.4}$$

$$1 = h(x_0^+, t) = h(x_0^-, t) \, . \tag{2.5}$$

These four constraints will be collectively referred to as jump conditions, since p will have a jump discontinuity at each point where $h = 1$. For a given a number of jumps, the jump conditions and the no-flux boundary conditions give us enough constraints to determine a unique stationary solution. Note, however, that there is nothing to determine the number of jumps (in general this will depend on the initial conditions of the system), or to guarantee that a stationary solution exists that satisfies all the constraints (we will see an example of this non-existence later). We may, however, concatenate copies of a stationary solution to construct a new solution on a larger domain. With this in mind, the rest of this paper will focus on solutions with a single jump discontinuity.

More generally, for a moving interface the condition $\tau p_t = 0$ may not hold. In this case a Dirac delta may appear in the p_t term in equation (1.5*a*), which will contribute an additional term when we integrate around $x_0(t)$. To account for this, we will re-integrate the equation more carefully. Suppose p takes the form $p = A(t)H(x - x_0(t)) + \hat{p}(x, t)$, where $x_0(t)$ is the location of the interface, H is a Heaviside function, and $\hat{p}(x, t)$ is continuous.

https://doi.org/10.1017/S0956792518000013 Published online by Cambridge University Press

We then obtain

$$\tau \int_{x_0^-}^{x_0^+} p_t dx = \int_{x_0^-}^{x_0^+} (sp)_{xx} dx + \int_{x_0^-}^{x_0^+} p(1-p) dx \tag{2.6}$$

$$-\tau A(t) x_0'(t) = sp_x|_{x_0^-}^{x_0^+} \tag{2.7}$$

The other three jump conditions remain unchanged.

2.2 Solutions for $\tau = 0$, small D_h and large $D_\pm$

We now turn our attention to approximate solutions with one jump discontinuity. Setting $\tau = 0$, we recover the PDE for stationary p. We will not, however, assume the system as a whole is stationary. Consequently, p depends on time implicitly via the position of the jump discontinuity, $x_0(t)$. Since the exact solution for h does not lend itself to easy algebraic manipulation, we limit our consideration to the small diffusion case, $0 < D_h \ll 1$.

Solutions for h are obtained by matching approximate solutions constructed near $x_0(t)$ and away from $x_0(t)$. Away from $x_0(t)$, diffusion is very small, and so h is approximately equal to p (see Figure 2). To determine the behaviour of h around $x_0(t)$, we introduce inner variables,

$$h(x) = H(y), \quad y = \frac{x - x_0(s)}{\sqrt{D_h}}, \quad \hat{t} = \sqrt{D_h} t \tag{2.8}$$

so that (1.5b) becomes

$$-x_{0\hat{t}} H_y = H_{yy} + p - H. \tag{2.9}$$

In order to match with the solution away from x_0, we require that $H \to p\left(x_0^{\pm}\right)$ as $y \to \pm\infty$. At the jump $x = x_0$, we have

$$H\left(0^{\pm}\right) = 1 \text{ and } H'(0^+) = H'\left(0^-\right). \tag{2.10}$$

Solutions for h are defined piecewise on either side of the jump, and take the form

$$H = p + c_1 e^{r_1 y} + c_2 e^{r_2 y} \tag{2.11}$$

where r_1 and r_2 are roots of the characteristic equation $0 = r^2 + x_{0\hat{t}} r - 1$,

$$r_1 = \frac{-x_{0\hat{t}} + \sqrt{x_{0\hat{t}}^2 + 4}}{2} \text{ and } r_2 = \frac{-x_{0\hat{t}} - \sqrt{x_{0\hat{t}}^2 + 4}}{2} \tag{2.12}$$

with $r_1 > 0$ and $r_2 < 0$. We will use the subscripts l and r to denote solutions to the left and right of $x_0(t)$. Applying the limiting conditions $H \to p_l$ as $y \to -\infty$ and $H \to p_r$ as $y \to +\infty$, we have $H_l = p_l + c_1 e^{r_1 y}$ and $H_r = p_r + c_2 e^{r_2 y}$. The jump conditions (2.10) then yield

$$p_l + c_1 = p_r + c_2 = 1, \quad c_1 r_1 = c_2 r_2 \,. \tag{2.13}$$

https://doi.org/10.1017/S0956792518000013 Published online by Cambridge University Press

Eliminating c_1, c_2 then yields

$$\frac{p_l - p_r}{1 - p_r} = \frac{r_1 - r_2}{r_1} = \frac{2\sqrt{x_{0\hat{t}}^2 + 4}}{-x_{0\hat{t}} + \sqrt{x_{0\hat{t}}^2 + 4}}. \tag{2.14}$$

Solving for x_0', we finally obtain the equation for the motion of the interface,

$$x_0'(t) = \sqrt{D_h}\frac{p_l(x_0) + p_r(x_0) - 2}{\sqrt{1 - p_r(x_0)}\sqrt{p_l(x_0) - 1}}. \tag{2.15}$$

In constructing an equation of motion for the jump x_0, we have effectively eliminated h from the system. The motion of x_0 does not depend explicitly on h, and all that is needed to specify the value of p is the location of x_0. In principle, this can be done by solving for p in outer region in terms of the Jacobi elliptic functions, resulting in a set of transcendental equations. However, we can obtain more explicit results if we assume D_+ and D_- are large. In this case, the diffusive term dominates, so $p(x)$ is approximately piecewise constant. Expanding $p(x)$ in terms of a Taylor series at either end of the domain, we then obtain the following approximations

$$\begin{aligned} p_l(x) &\sim p_{l0} + p_{l2}x^2 && \text{for } x < x_0\ , \\ p_r(x) &\sim p_{r0} + p_{r2}(x-1)^2 && \text{for } x > x_0\ . \end{aligned}$$

Without loss of generality, assume $p_{l0} > p_{r0}$ (see Figure 2) i.e., $s(h) = D_+$ in the left of x_0, and let

$$s_0 := \frac{D_+}{D_-} < 1. \tag{2.16}$$

The jump conditions (2.2) and (2.3) then yield

$$\frac{p_{r0}}{p_{l0}} = s_0 = \frac{p_{r2}(x_0 - 1)}{p_{l2}x_0}.$$

Substituting the approximations for p into (1.5a), assuming $p_t\tau = 0$ yields two more conditions:

$$\begin{aligned} 0 &= 2D_+p_{l2} + p_{l0}(1 - p_{l0}), \\ 0 &= 2D_-p_{r2} + p_{r0}(1 - p_{r0}). \end{aligned}$$

Eliminating p_{r2}, p_{l2} then yields

$$s_0\frac{x_0 - 1}{x_0} = \frac{p_{l0} - 1}{p_{r0} - 1} \tag{2.17}$$

so that

$$p_{l0} = \frac{s_0x_0 - s_0 - x_0}{s_0^2x_0 - s_0^2 - x_0}; \quad p_{r0} = s_0p_{0l}. \tag{2.18}$$

Upon substituting (2.18) into (2.15), we finally obtain the full equation of motion of the interface. Note that when computing p, we assumed that the term τp_t can be dropped. Since the interface speed is of $O(D_h^{1/2})$, this assumption is valid as long as $\tau D_h^{-1/2} \ll 1$. We summarize.

https://doi.org/10.1017/S0956792518000013 Published online by Cambridge University Press

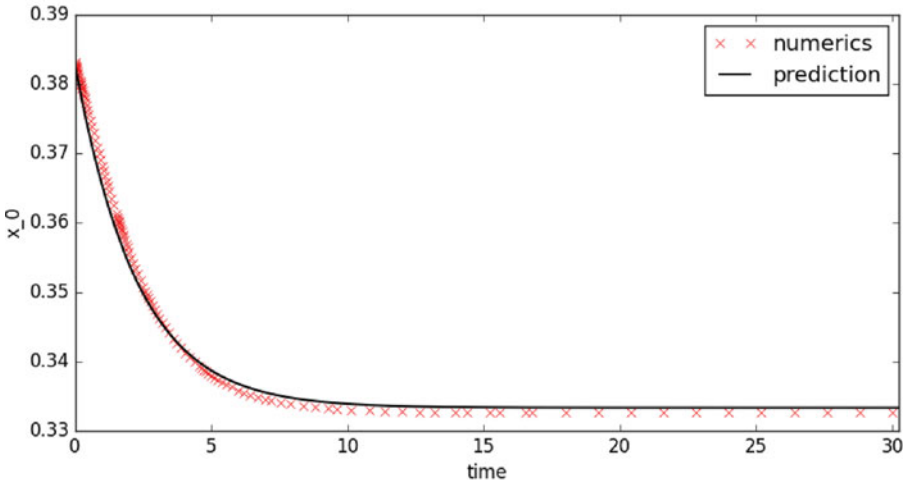


FIGURE 3. Motion of the front as predicted by the ODE (in black) compared to simulation results (red crosses). Simulation parameter are $D_h = 0.01$, $\tau = 0$, and with $s(h)$ as given in (1.4) with $D_+ = 50$, $D_- = 100$, $\delta = 0.001$.

Proposition 1 *Suppose*

$$D_- > D_+ \gg 1,\ D_h \ll 1 \text{ and } \tau \ll O(D_h^{-1/2}). \tag{2.19}$$

Then there is a time-dependent solution to (1.5) consisting of a single interface at $x_0(t)$, which has the following asymptotic form,

$$p(x) = \begin{cases} \dfrac{s_0 x_0 - s_0 - x_0}{s_0^2 x_0 - s_0^2 - x_0} & x \leqslant x_0 \\ \dfrac{s_0^2 x_0 - s_0^2 - s_0 x_0}{s_0^2 x_0 - s_0^2 - x_0} & x > x_0 \end{cases}, \qquad h \sim p \text{ for } |x - x_0| \gg O(1/\sqrt{D_h}). \tag{2.20}$$

where $s_0 = D_+/D_-$ and where x_0 satisfies the ODE

$$x_0'(t) = \sqrt{D_h}\frac{s_0(1 - x_0(t)) - x_0(t)}{\sqrt{s_0 x_0(t)(1 - x_0(t))}}. \tag{2.21}$$

Figure 3 shows a comparison between the asymptotic formula (2.21) and the full numerical simulation of (2.21). The trajectory of $x_0(t)$ in the simulation matches the behaviour predicted by the equation of motion. The interface settles to $x_0 \approx 0.333$ that appears to be stable. To validate this, note that ODE (2.21) admits a steady state

$$x_0 = \frac{s_0}{s_0 + 1} \in (0, 1), \tag{2.22}$$

https://doi.org/10.1017/S0956792518000013 Published online by Cambridge University Press

in full agreement with numerics of Figure 3. The associated eigenvalue of linearization around this steady state is given by

$$\lambda = -\sqrt{D_h}\frac{(1+s_0)^2}{s_0} \tag{2.23}$$

and is negative, showing the stability of the interface, again in agreement with full numerics of Figure 3.

3 Steady state and its stability

The fully analytical formula for the interface motion (2.21) was possible by making assumptions (2.19). Under these assumptions, the interface moves towards a *stable* steady state (2.22). When these conditions are relaxed, in particular if D_h and/or τ are no longer small, instabilities may occur. However, under these relaxed conditions, the construction of a moving interface becomes analytically intractable. Instead, we take a different approach: we compute the steady state and its linearization.

Let us construct the steady state under a relaxed assumption that D_h is not necessary small, while $D_\pm$ are still large (for the steady state, $p_t = 0$, so that τ can take any value; it affects stability but not the steady state). The steady state for $p(x)$ is then the same as given in Proposition 1. On the other hand, assuming h is stationary, equation (1.5*b*) reduces to

$$0 = D_h h_{xx} + p - h,$$

whose solution is given by

$$h = \begin{cases} p_{l0} + c_1 \cosh\left(\sqrt{\frac{1}{D_h}}x\right), & x < x_0 \\ p_{r0} + c_2 \cosh\left(\sqrt{\frac{1}{D_h}}(x-1)\right), & x > x_0 \end{cases}. \tag{3.1}$$

The jump conditions (2.4) and (2.5) then yield

$$\begin{aligned} 1 &= p_{l0} + c_1 \cosh\left(\sqrt{\frac{1}{D_h}}x_0\right), \\ 1 &= p_{r0} + c_2 \cosh\left(\sqrt{\frac{1}{D_h}}(x_0-1)\right), \\ c_1 \sinh\left(\sqrt{\frac{1}{D_h}}x_0\right) &= c_2 \sinh\left(\sqrt{\frac{1}{D_h}}(x_0-1)\right). \end{aligned}$$

Substituting into (2.17), we finally obtain

$$s_0\frac{x_0-1}{x_0} = \frac{\tanh\left(\sqrt{\frac{1}{D_h}}(x_0-1)\right)}{\tanh\left(\sqrt{\frac{1}{D_h}}x_0\right)}. \tag{3.2}$$

https://doi.org/10.1017/S0956792518000013 Published online by Cambridge University Press

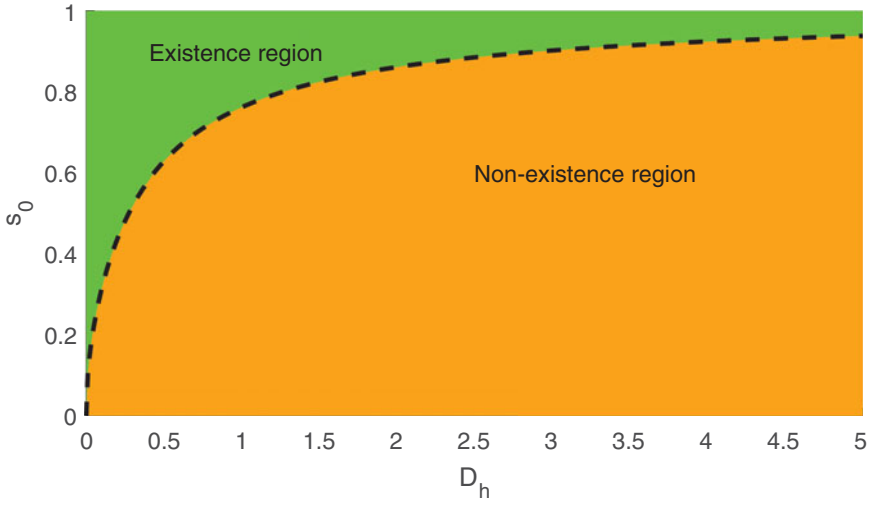


FIGURE 4. Existence/non-existence of interface solutions as a function of D_h versus $s_0 = D_+/D_-$. The dashed boundary is given by $s_0 = D_h^{1/2}\tanh(D_h)$. Solutions exist for s_0 above this boundary.

Solving this equation determines the stationary value of x_0, which in turn determines both p and h. When D_h is small, we may approximate $\frac{\tanh\left(\sqrt{\frac{1}{D_h}}(x_0-1)\right)}{\tanh\left(\sqrt{\frac{1}{D_h}}x_0\right)} \sim -1$ so that (3.2) reduces to $s_0 \sim \frac{x_0}{1-x_0}$, which is equivalent to (2.22). More generally, observe that the function $x_0 \to \tanh\left(\sqrt{\frac{1}{D_h}}x_0\right)/x_0$ is decreasing for $x_0 \geqslant 0$ and therefore the function $F(x_0) = \frac{\tanh\left(\sqrt{\frac{1}{D_h}}(1-x_0)\right)/(1-x_0)}{\tanh\left(\sqrt{\frac{1}{D_h}}x_0\right)/x_0}$ is increasing as a function of $x_0 \in [0,1]$, for any D_h. Moreover, $F(0) = \tanh\left(\sqrt{\frac{1}{D_h}}\right)\sqrt{D_h} < 1$, whereas $F(1) \sim \coth\left(\sqrt{\frac{1}{D_h}}\right)/\sqrt{D_h} > 1$. Therefore, the solution to (3.2) exists and is unique if and only if $F(1) > s_0$, that is, if and only $\tanh\left(\sqrt{\frac{1}{D_h}}\right)\sqrt{D_h} < s_0$, see Figure 4. We summarize this as follows.

Proposition 2 *Suppose $D_- > D_+ \gg 1$, and let $s_0 = \frac{D_+}{D_-} < 1$. Suppose that $s_0 > \tanh\left(\sqrt{\frac{1}{D_h}}\right)\sqrt{D_h}$. Then, the system (1.5) admits a non-trivial steady-state solution with $p(x)$ given by (2.20) and $h(x)$ given by (3.1), where x_0 is the unique solution to (3.2). If in addition, $D_h \ll 1$, then*

$$x_0 \sim \frac{s_0}{s_0+1}$$

and p simplifies to

$$p(x) \sim \begin{cases} \dfrac{2}{s_0+1} & x \leqslant x_0 \\ \dfrac{2s_0}{s_0+1} & x > x_0. \end{cases} \tag{3.3}$$

No solution to (3.2) (and therefore no steady state) exists if $s_0 < \tanh\left(\sqrt{\frac{1}{D_h}}\right)\sqrt{D_h}$.

https://doi.org/10.1017/S0956792518000013 Published online by Cambridge University Press

3.1 Linearization and an eigenvalue problem

We now linearize around the steady state constructed in Proposition 2 as follows:

$$p(x,t) = p_s(x) + e^{\lambda t}\phi(x), \quad h(x,t) = h_s(x) + e^{\lambda t}\psi(x).$$

This leads to the following eigenvalue problem:

$$\lambda\tau\phi(x) = D_{\pm}\phi''(x) + \phi(x)\,(1 - 2p_s(x)) \ , \tag{3.4}$$

$$\lambda\psi(x) = D_h\psi''(x) + \phi(x) - \psi(x) \ , \tag{3.5}$$

with no-flux boundary conditions for ϕ and ψ. Deriving jump conditions for the eigenvalue problem, however, requires more care. There are two ways to carry out the calculation: by integrating the equations across the jump, as we did for the original system, or by linearizing the original jump conditions. We begin with the former.

3.2 Jump conditions via integration

We assume that ϕ takes the form $\phi(x) = \hat{\phi}(x) + c\delta(x - x_0)$, where c is a constant to be deterimed, δ is a Dirac delta, and $\hat{\phi}$ is a (potentially discontinuous) function. We also assume ψ has no Dirac delta component.

Integrating (3.5) on a small interval around x_0, we obtain

$$\lambda\int_{x_0^-}^{x_0^+}\psi dx = D_h\int_{x_0^-}^{x_0^+}\psi_{xx}dx + \int_{x_0^-}^{x_0^+}\phi dx - \int_{x_0^-}^{x_0^+}\psi dx \to 0$$

$$0 = D_h\psi'\big|_{x_0^-}^{x_0^+} + c \ .$$

Premultiplying (3.5) by x and performing integration by parts, we derive

$$\lambda\int_{x_0^-}^{x_0^+}x\psi dx = D_h\int_{x_0^-}^{x_0^+}x\psi_{xx}dx + \int_{x_0^-}^{x_0^+}x\phi dx - \int_{x_0^-}^{x_0^+}x\psi dx \to 0$$

$$0 = -x_0c - D_h\psi\big|_{x_0^-}^{x_0^+} + cx_0$$

$$0 = \psi\big|_{x_0^-}^{x_0^+} \ .$$

Integrating (3.4) requires care in taking limits. Begin by integrating over $(x_0 - \Delta, x_0 + \Delta)$, where Δ is some small constant. We temporarily replace s by a sufficiently continuous sigmoid that switches value in some ε-neighbourhood around x_0 (i.e., $s(h)$ is approximately constant outside $(x_0 - \varepsilon, x_0 + \varepsilon)$). Observe that

$$s(h)p(x,t) \approx s(h_s)p_s(x) + p_s(x)s'(h_s)\psi(x)e^{\lambda t} + s(h_s)\phi(x)e^{\lambda t} \ ,$$

and adjust the linearization accordingly to obtain

$$\lambda\tau\phi(x) = \big(\psi(x)s'(h_s)p_s(x) + s(h_s)\phi(x)\big)_{xx} + \phi(x)\,(1 - 2p_s(x)) \ . \tag{3.6}$$

https://doi.org/10.1017/S0956792518000013 Published online by Cambridge University Press

After integrating, we will take the limit $\Delta \to 0$, and assume $\varepsilon \ll \Delta$. We also adopt the notation $f^{\pm} := f(x_0^{\pm})$. Integrating (3.6) and taking the aforementioned limit yields

$$\begin{aligned}\tau\lambda \int_{x_0-\Delta}^{x_0+\Delta} \phi dx &= \int_{x_0-\Delta}^{x_0+\Delta} (\psi s'(h_s)p_s + s(h_s)\phi)_{xx} dx + \int_{x_0-\Delta}^{x_0+\Delta} \phi(1-2p_s)dx \\ \tau\lambda c &= \lim_{\Delta\to 0} (\psi s'(h_s)p_s + s(h_s)\phi)_x|_{x_0-\Delta}^{x_0+\Delta} + c(1-p_s^+ - p_s^-) \\ \tau\lambda c &= s(h_s)\phi'|_{x_0^-}^{x_0^+} + c(1-p_s^+ - p_s^-) \ .\end{aligned}$$

Similarly, premultiplying (3.6) by x and integrate by parts, we obtain

$$0 = s(h_s)\phi|_{x_0^-}^{x_0^+} \ .$$

Finally, premultiply (3.6) by x^2 and integrate by parts twice, we obtain

$$c = \frac{\psi(x_0)}{h_s'(x_0)}(p_s^+ - p_s^-) \ .$$

This last equation can be used to eliminate c, yielding the final jump conditions for the eigenvalue problem:

$$0 = s\phi'|_{x_0^-}^{x_0^+} + \frac{\psi(x_0)}{h_s'(x_0)}(p_s^+ - p_s^-)\left(1 - p_s^+ - p_s^- - \tau\lambda\right) \ , \tag{3.7a}$$

$$0 = s\phi|_{x_0^-}^{x_0^+} \ , \tag{3.7b}$$

$$0 = D_h\psi'|_{x_0^-}^{x_0^+} + \frac{\psi(x_0)}{h_s'(x_0)}(p_s^+ - p_s^-) \ , \tag{3.7c}$$

$$0 = \psi|_{x_0^-}^{x_0^+} \ . \tag{3.7d}$$

3.3 Jump conditions via linearization

We will now derive these equations by linearizing the matching conditions from the original system. Begin by noting that in the perturbed regime x_0 may vary with time. Because of this, we will need to linearize (2.7) rather than (2.2).

We linearize as before, taking $p(x,t) = p_s(x) + \phi(x)e^{\lambda t}$ and $h(x,t) = h_s(x) + \psi(x)e^{\lambda t}$. Since the location of the jump will change, we also perturb the interface location $x_0(t) = x_{0s} + \theta e^{\lambda t}$. As before, we split p and h into left and right components, denoted h_l, h_r, etc.

Expanding $h_l(x_0,t)$ and discarding higher order terms, we obtain

$$h_l(x_0,t) \approx 1 + e^{\lambda t}\left(\theta h_{sl}'(x_{0s}) + \psi_l(x_{0s})\right) \ .$$

We do the same for h_r, and substitute into (2.5). Recalling that $h_{sl}'(x_0) = h'_{sr}(x_0)$, this then yields

$$\psi_l(x_{0s}) = -\theta h'_{sl}(x_{0s}) = \psi_r(x_{0s}) \ .$$

https://doi.org/10.1017/S0956792518000013 Published online by Cambridge University Press

Similarly, expanding $\partial_x h_l(x_0, t)$ yields

$$\partial_x h_l(x_0, t) \approx h'_{sl}(x_{0s}) + e^{\lambda t}\left(\theta h''_{sl}(x_0) + \psi'_l(x_0)\right) \ .$$

Substituting into (2.4) and simplifying yields

$$\psi'|_{x_{0s}^-}^{x_{0s}^+} = \theta \frac{\alpha}{D_h} p_s|_{x_{0s}^-}^{x_{0s}^+} \ .$$

Repeating this procedure for p and $\partial_x p$ and substitute into (2.7) and (2.3), we obtain

$$0 = s\phi|_{x_{0s}^-}^{x_{0s}^+} \ ,$$
$$0 = s\phi'|_{x_{0s}^-}^{x_{0s}^+} + \theta\left(\tau\lambda(p_s^+ - p_s^-) + sp''_s|_{x_{0s}^-}^{x_{0s}^+}\right) \ .$$

Eliminating θ, and reverting to the previous notation $x_{0s} \to x_0$, we recover

$$0 = s\phi'|_{x_0^-}^{x_0^+} - \frac{\psi(x_0)}{h'_e(x_0)}\left(\tau\lambda(p_s^+ - p_s^-) + sp'_s|_{x_0^-}^{x_0^+}\right) \ , \tag{3.8a}$$

$$0 = s\phi|_{x_0^-}^{x_0^+} \ , \tag{3.8b}$$

$$0 = D_h\psi'|_{x_0^-}^{x_0^+} + \frac{\psi(x_0)}{h'_e(x_0)} p_s|_{x_0^-}^{x_0^+} \ , \tag{3.8c}$$

$$0 = \psi|_{x_0^-}^{x_0^+} \ . \tag{3.8d}$$

At first glance, the first of these may appear different to equations (3.7). However, using the fact that $sp''_s = -p_s(1 - p_s)$, we can show that these are, in fact, equivalent.

3.4 Solutions to the eigenvalue problem for large $D_\pm$

Having adequately set up the eigenvalue problem, we now solve the system in the limit of large $D_\pm$. In this case, the steady state is approximated by a piece-wise linear function (see Proposition 2), and the resulting eigenvalue problem can be simplified as follows. In keeping with our previous notation, we define ϕ_l, ϕ_r, etc. Recall that, to leading order, $p_{sl}(x) = p_{l0}$. Let $\omega_l = \frac{1}{D_+}(1 - 2p_{l0} - \tau\lambda)$. Solving (4.1) in the left of the domain, we obtain $\phi_l(x) = c_{l1}\cos(\sqrt{\omega_l}x)$, where c_{l1} is some constant to be determined. A similar solutions can be found for the right part of the domain.

Substituting int (3.5) yields a differential equations for ψ_l;

$$\psi''_l(x) = -\frac{c_{l1}}{D_h}\cos(\sqrt{\omega_l}x) + \frac{1+\lambda}{D_h}\psi_l(x) \ .$$

It has the following solution,

$$\psi_l(x) = \frac{c_{l1}}{1 + \lambda + D_h\omega_l}\cos(\sqrt{\omega_l}x) + c_{l2}\cosh\left(\sqrt{\frac{1+\lambda}{D_h}}x\right) \ ,$$

where c_{l2} is a constant.

https://doi.org/10.1017/S0956792518000013 Published online by Cambridge University Press

We can find similar solutions for the right of the domain. We substitute these solutions into equations (3.7). To simplify notation, let $k = \frac{p_s^+ - p_s^-}{h_s'(x_0)}\left(1 - p_s^+ - p_s^- - \tau\lambda\right)$. This results in the equations

$$\begin{aligned}
0 =& - D_- c_{r1}\sqrt{\omega_r}\sin(\sqrt{\omega_r}(x_0-1)) + D_+ c_{l1}\sqrt{\omega_l}\sin(\sqrt{\omega_l}x_0) \\
&+ k\left(\frac{c_{l1}}{1+\lambda+D_h\omega_l}\cos(\sqrt{\omega_l}x_0) + c_{l2}\cosh\left(\sqrt{\frac{1+\lambda}{D_h}}x_0\right)\right), \\
0 =& D_- c_{r1}\cos(\sqrt{\omega_r}(x_0-1)) - D_+ c_{l1}\cos(\sqrt{\omega_l}x_0), \\
0 =& \frac{c_{r1}}{1+\lambda+D_h\omega_r}\cos(\sqrt{\omega_r}(x_0-1)) + c_{r2}\cosh\left(\sqrt{\frac{1+\lambda}{D_h}}(x_0-1)\right) \\
&- \frac{c_{l1}}{1+\lambda+D_h\omega_l}\cos(\sqrt{\omega_l}x_0) - c_{l2}\cosh\left(\sqrt{\frac{1+\lambda}{D_h}}x_0\right),
\end{aligned}$$

and

$$\begin{aligned}
0 =& - \frac{c_{r1}\sqrt{\omega_r}}{1+\lambda+D_h\omega_r}\sin(\sqrt{\omega_r}(x_0-1)) + c_{r2}\sqrt{\frac{1+\lambda}{D_h}}\sinh\left(\sqrt{\frac{1+\lambda}{D_h}}(x_0-1)\right) \\
&+ \frac{c_{l1}\sqrt{\omega_l}}{1+\lambda+D_h\omega_l}\sin(\sqrt{\omega_l}x_0) - c_{l2}\sqrt{\frac{1+\lambda}{D_h}}\sinh\left(\sqrt{\frac{1+\lambda}{D_h}}x_0\right) \\
&+ \frac{1}{D_h h_s'(x_0)}(p_s^+ - p_s^-)\left(\frac{c_{l1}}{1+\lambda+D_h\omega_l}\cos(\sqrt{\omega_l}x_0) + c_{l2}\cosh\left(\sqrt{\frac{1+\lambda}{D_h}}x_0\right)\right).
\end{aligned}$$

Written in matrix notation, we have

$$M\begin{bmatrix} c_{l1} \\ c_{r1} \\ c_{l2} \\ c_{r2} \end{bmatrix} = \begin{bmatrix} 0 \\ 0 \\ 0 \\ 0 \end{bmatrix}$$

where M is given by

$$M = \begin{bmatrix}
M_{11} & -D_-\sqrt{\omega_r}\sin(\sqrt{\omega_r}(x_0-1)) & k\cosh(Bx_0) & 0 \\
-D_+\cos(\sqrt{\omega_l}x_0) & D_-\cos(\sqrt{\omega_r}(x_0-1)) & 0 & 0 \\
-A_l\cos(\sqrt{\omega_l}x_0) & A_r\cos(\sqrt{\omega_r}(x_0-1)) & -\cosh(Bx_0) & \cosh(B(x_0-1)) \\
M_{41} & -\sqrt{\omega_r}A_r\sin(\sqrt{\omega_r}(x_0-1)) & M_{43} & B\sinh(B(x_0-1))
\end{bmatrix}, \tag{3.9}$$

$$\begin{aligned}
M_{11} &= D_+\sqrt{\omega_l}\sin(\sqrt{\omega_l}x_0) + kA_l\cos(\sqrt{\omega_l}x_0) \\
M_{41} &= \sqrt{\omega_l}A_l\sin(\sqrt{\omega_l}x_0) + \frac{(p_s^+ - p_s^-)}{D_h h_s'(x_0)}A_l\cos(\sqrt{\omega_l}x_0) \\
M_{34} &= -B\sinh(Bx_0) + \frac{(p_s^+ - p_s^-)}{D_h h_s'(x_0)}\cosh(Bx_0)
\end{aligned}$$

https://doi.org/10.1017/S0956792518000013 Published online by Cambridge University Press

$$A_l = \frac{1}{1+\lambda+D_h\omega_l}, \quad A_r = \frac{1}{1+\lambda+D_h\omega_r} \; B = \sqrt{\frac{1+\lambda}{D_h}}.$$

In order to have non-trivial solutions, we require that $\det M = 0$. Written in full, this determinant is

$$\begin{aligned}
0 = \det M = & -D_+D_-\sqrt{\omega_r}B\cos(\sqrt{\omega_l}x_0)\sin(\sqrt{\omega_r}(x_0-1))\sinh(B) \\
& + \frac{p_s^+ - p_s^-}{D_h h_s'(x_0)} D_+D_-\sqrt{\omega_r}\cos(\sqrt{\omega_l}x_0)\sin(\sqrt{\omega_r}(x_0-1))\cosh(B(x_0-1))\cosh(Bx_0) \\
& - A_rBD_+k\cos(\sqrt{\omega_l}x_0)\cosh(Bx_0)\cos(\sqrt{\omega_r}(x_0-1))\sinh(B(x_0-1)) \\
& - D_+k\sqrt{\omega_r}A_r\cos(\sqrt{\omega_l}x_0)\cosh(Bx_0)\cosh(B(x_0-1))\sin(\sqrt{\omega_r}(x_0-1)) \\
& + D_-D_+\sqrt{\omega_l}B\cos(\sqrt{\omega_r}(x_0-1))\sin(\sqrt{\omega_l}x_0)\sinh(B) \\
& - \frac{p_s^+ - p_s^-}{D_h h_s'(x_0)} D_-D_+\sqrt{\omega_l}\cos(\sqrt{\omega_r}(x_0-1))\sin(\sqrt{\omega_l}x_0)\cosh(B(x_0-1))\cosh(Bx_0) \\
& + D_-kA_lB\cos(\sqrt{\omega_r}(x_0-1))\cos(\sqrt{\omega_l}x_0)\sinh(B) \\
& + D_-kA_lB\cos(\sqrt{\omega_r}(x_0-1))\cosh(Bx_0)\cos(\sqrt{\omega_l}x_0)\sinh(B(x_0-1)) \\
& + D_-k\sqrt{\omega_l}A_l\cos(\sqrt{\omega_r}(x_0-1))\cosh(Bx_0)\cosh(B(x_0-1))\sin(\sqrt{\omega_l}x_0)\,.
\end{aligned} \tag{3.10}$$

Thus, the eigenvalue problem reduces to finding the roots of this expression. While this is analytically intractable, we can nevertheless find roots numerically, tracking the movement of the first eigenvalues (see Figure 5). This analysis reveals that Hopf bifurcations may occur when one of D_h or τ is sufficiently large. Simulations at appropriate parameter values reveal the expected oscillatory behaviour (see Figure 6).

We double-checked these calculations by solving the eigenvalue problem (3.5), (3.6) directly. To do this, we replaced $s(h)$ by a sharp sigmoid. We first solved for the steady state using a boundary value problem `bvp45` in Matlab. We then discretized the eigenvalue problem (3.5), (3.6) using finite differences in space. This converts the problem to a matrix eigenvalue problem where the matrix in question is very sparse. We then used matlab to readily find the eigenvalues of the resulting matrix. The resulting computations confirmed the validity of (3.10).

3.5 Revisiting stability in the small D_h, $\tau = 0$ regime

While the equation governing the eigenvalues in the large s case is generally intractable, we should expect it to simplify considerably when D_h is small and $\tau = 0$. After all, we have already shown that this limiting case is stable and has a relatively simple eigenvalue. Expanding (3.10) for small D_h and large $D_\pm$ yields, after a lot of algebra,

$$0 = (s_0+1)\,D_-\left(\sqrt{D_h}\,(s_0+1)^2 + 2s_0\,(1+\lambda)\right)\sqrt{1+\lambda} - (2\lambda+2)\,D_-s_0(s_0+1).$$

https://doi.org/10.1017/S0956792518000013 Published online by Cambridge University Press

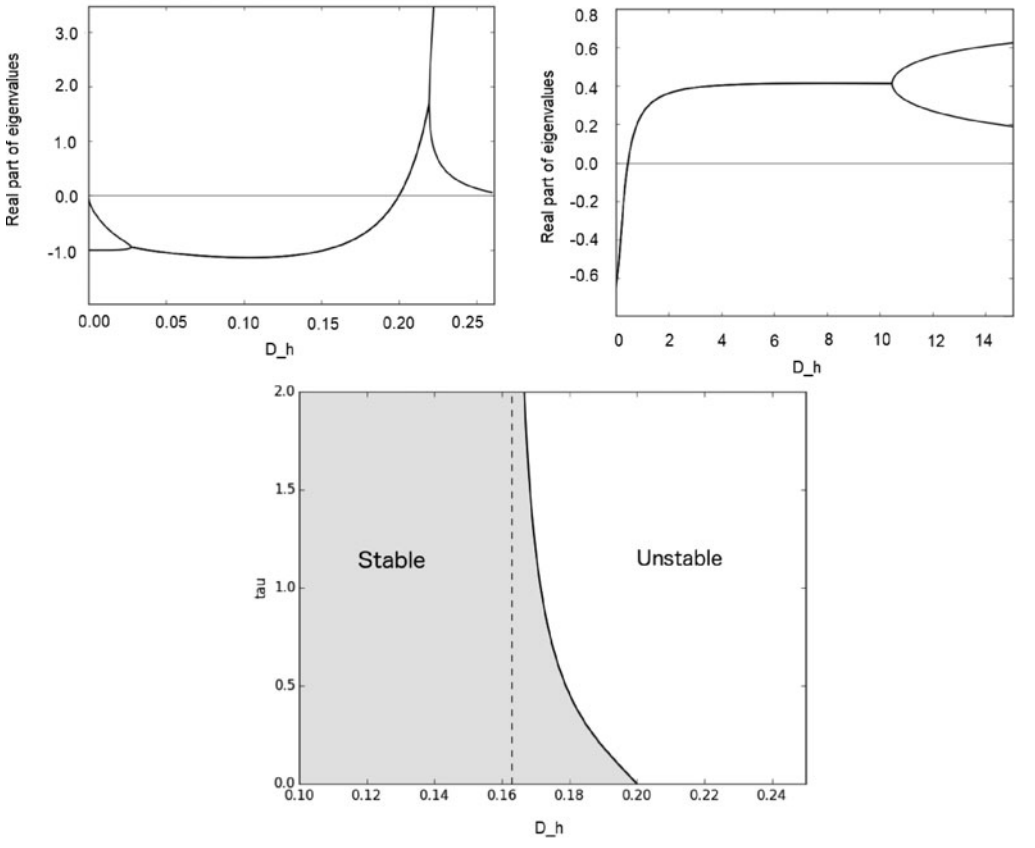


FIGURE 5. Plotting the real part of the first two eigenvalues as a function of D_h with $\tau = 0$ (top left), and as a function of τ with $D_h = 0.18$ (top right), with $D_+ = 50$, $D_- = 100$. Notice in the former that as D_h becomes large, the first eigenvalue grows very quickly. This apparent asymptote corresponds to the onset of non-existence of single-jump solutions. At intermediate D_h values the first two roots become a complex pair, and the system undergoes a Hopf bifurcation at $D_h \approx 0.20001$. For small D_h values, the first two roots are again real, but remain negative. In the top right plot, a Hopf bifurcation occurs at $\tau \approx 0.45885$. As τ is increased further, the complex pair splits into real roots, and the second root approaches zero (not shown). The solid line in the bottom figure tracks the value of τ that produces a Hopf bifurcation for any given value of D_h ($D_+ = 50$, $D_- = 100$). To the left and right of this curve, solutions are stable and unstable, respectively. The curve has a vertical asymptote at $D_h \approx 0.16296$.

Solving for λ, we then find

$$\lambda = -1\ ,$$

$$\lambda = \frac{1}{2}\frac{-\sqrt{D_h}\,(s_0+1)^2 - \sqrt{s_0^2 - 2\sqrt{D_h}\,(s_0+1)^2\,s_0} - s_0}{s_0}\ ,$$

$$\lambda = \frac{1}{2}\frac{-\sqrt{D_h}\,(s_0+1)^2 + \sqrt{s_0^2 - 2\sqrt{D_h}\,(s_0+1)^2\,s_0} - s_0}{s_0}\ .$$

https://doi.org/10.1017/S0956792518000013 Published online by Cambridge University Press

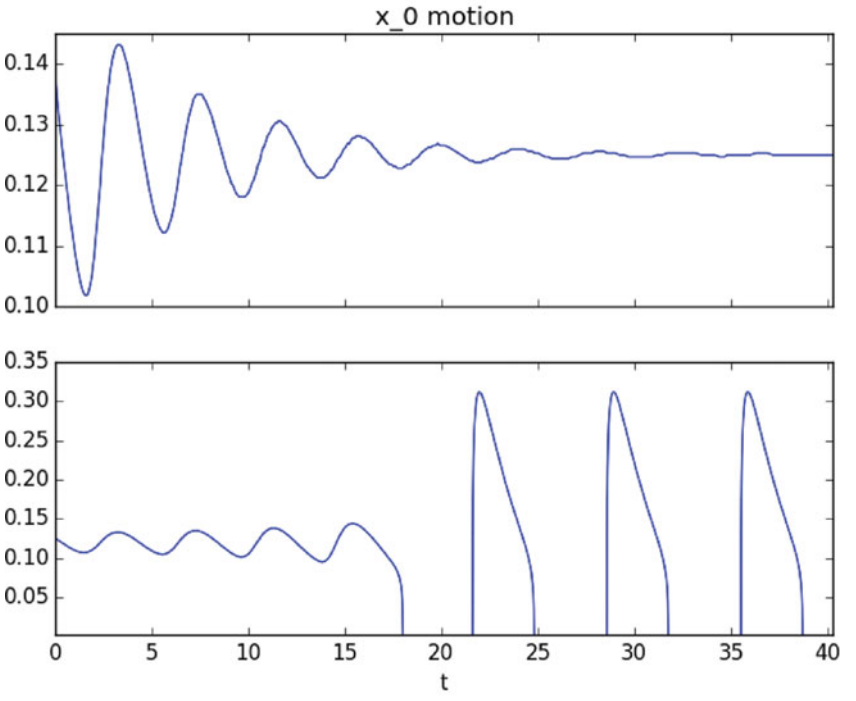


FIGURE 6. Plots comparing the motion of x_0 in the linearly stable ($D_h = 0.199$, top) and linearly unstable ($D_h = 0.203$, bottom) regimes. In both cases $\tau = 0$, and $s(h)$ is given as in (1.4) with $D_+ = 50$, $D_- = 100$ and $\delta = 0.001$. In each plot, the steady-state solution was perturbed, and the location of x_0 tracked as the solution evolved. In the stable case, the location of x_0 exhibits damped oscillations consistent with the predicted eigenvalues. In the unstable case, the oscillations grow until x_0 drifts to the edge of the domain, at which point the solution collapses to an approximately constant and homogeneous profile ($t \approx 18$). This is followed by repeated spontaneous emergence of structure via Turing instability, punctuated by collapse to a nearly constant solution.

Finally, expanding $\sqrt{s_0^2 - 2\sqrt{D_h}(s_0+1)^2 s_0} \sim s_0 - \sqrt{D_h}(s_0+1)^2$, we find that these two last roots are $\lambda \sim -1$ and $\lambda \sim -\sqrt{D_h}\frac{(s_0+1)^2}{s_0}$. This recovers the formula (2.23) obtained through linearization of the equations of motion of the interface. Notice also that in Figure 5, the second eigenvalue goes to -1 as $D_h \to 0$, as predicted by this analysis.

4 Discussion

We have studied in detail interface patterns of the PDE model (1.5) proposed in [17]. In the limit of sharp step-like diffusion function $s(h)$, these solutions contain jump discontinuities, similar to a square wave. We focused our attention on solutions with a single jump discontinuity, and derived, assuming the diffusion of AHL D_h was small, an equation of motion for a discontinuity that is not at equilibrium. The equation of motion was able to predict results from numerical simulations. From this equation of motion, we were able to deduce that such solutions are stable when diffusion of bacteria is large.

https://doi.org/10.1017/S0956792518000013 Published online by Cambridge University Press

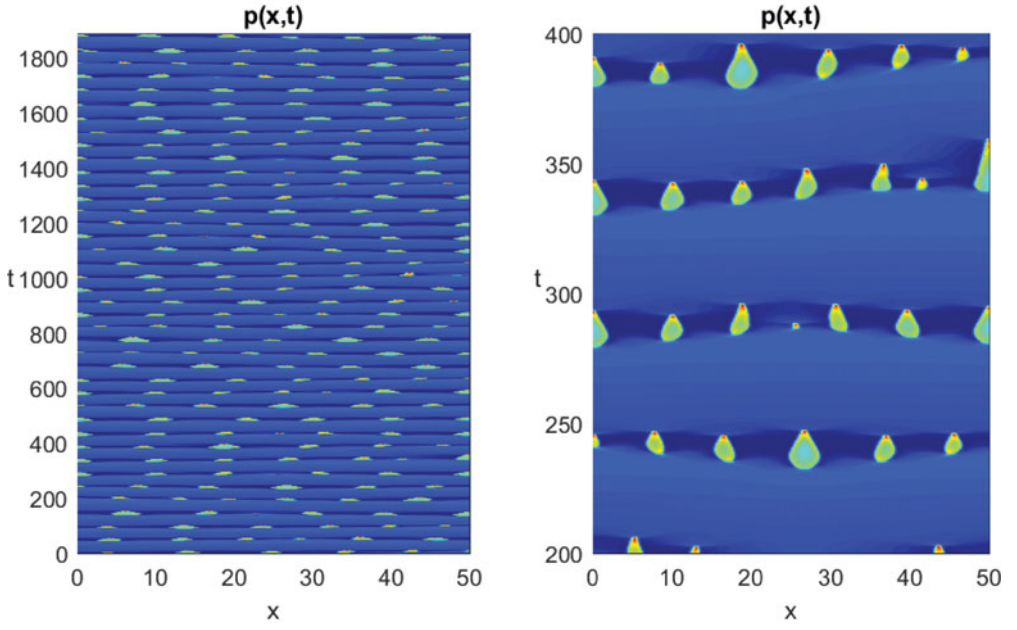


FIGURE 7. Complex, chaotic dynamics for the system (1.5) with $x \in [0, 50]$, $D_h = 1.5$, $\tau = 1$, and with $s(h)$ as given in (1.4) with $D_+ = 2$, $D_- = 40$, $\delta = 0.1$. Right panel is a zoom of the left panel. The interfaces are being continuously created and destroyed.

We then turned our attention to stability in a more general case (lifting the requirement that D_h be small, but maintaining the requirement that there be only one jump discontinuity), and derived an associated eigenvalue problem, whose solution reduces to finding the roots of a transcendental equation. Solving this equation numerically, we demonstrated the existence of a Hopf bifurcation, which was also confirmed with numerical simulations of the original PDE. Finally, by expanding the transcendental equation for small D_h, we re-obtained the stability of the interface in this case.

The stable interface solutions we obtained are markedly different from that described in [17]. Though they used the same model, their choice of parameters was such that only transient patterns could be created; any structure that emerged eventually collapsed to the trivial constant state. To obtain the type of sustained pattern observed in experiment, their group developed a three-component PDE model [13]. Most of the difference in behaviour can be attributed to the nature of the function $s(h)$. In this paper, we chose $s(h)$ to ensure that the system exhibited a Turing instability, and this choice ensured that any observed steady states would be non-constant. It remains an open question whether or not such stable steady states exist for more generic $s(h)$.

This work provides further evidence that non-linear diffusion can act as a pattern generation mechanism. While the methods used were largely ad hoc and relied heavily on approximation, the results obtained agree with numerical simulation and display internal consistency (several of the results can be derived via multiple methods). It is our hope that these results might act as a catalyst for further experiments, or as a starting point for anyone who wishes to pursue a more rigorous analysis.

https://doi.org/10.1017/S0956792518000013 Published online by Cambridge University Press

As we have shown, even a single interface can lead to complex dynamics provided that D_h or τ is sufficiently large: the Hopf instability causes the interface to merge with the boundary. Ever more complex dynamics, including apparently chaotic dynamics, can arise if the domain is sufficiently large to accommodate multiple unstable interfaces. An example of such dynamics is shown in Figure 7. Another potential mechanism forming complex patterns has been suggested in [18–22].

Unlike many other classical reaction–diffusion systems such as Gierer–Meinhardt model [23] Gray-Scott model [24] and the Brusselator [25, 26], the main driver of patterns for (1.5) is the state-dependent diffusion $s(h)$. The model has some resemblance to the logistic chemotaxis model introduced in [27, 28] which was shown to admit very complex pattern dynamics [18–22]. However, the mechanism behind pattern formation appears to be rather different. In particular, the primary driver of complex patterns in the logistic chemotaxis model is the fact that patterns tend to attract to each other, and merge with each-other [21, 22]. By contrast, in the model (1.5) the patterns are destabilized via a Hopf bifurcation. Seemingly chaotic type dynamics have been observed in *E. coli* populations. The present model provides an alternative suggestion for how the chaotic patterns can emerge.

A number of open problems remain. Figure 4 indicates that a Hopf bifurcation occurs *for any* value of τ (including $\tau = 0$) if D_h is sufficiently large. In particular, the curve in Figure 4(bottom) has a vertical asymptote which we computed purely numerically. The proof of these facts is missing completely. Further numerics indicate the presence of very complex behaviour in the unstable regime (i.e., sufficiently large D_h) when the domain is large enough. How does one characterize the stability of solutions with multiple discontinuities? What can be said of the case where $\tau \neq 0$? Can one derive similar results where $s(h)$ is a smooth curve? Numerical simulations show that similar patterns form even when $s(h)$ is a sigmoid curve with a gradual slope. Finally, what happens when we extend this model to more than one spatial dimension? In the experiments that motivated the creation of this model, researchers observed stable stripes and concentric circles, and preliminary simulations show that the model has a natural tendency to develop spots when evolved from a perturbed homogeneous state. We hope to address these questions in future work.

Acknowledgements

We would like to thank Andrew Rutenberg for discussions of the state-dependent Brownian motion. T. K. was supported by NSERC Discovery Grant no. RGPIN-33798 and Accelerator Supplement Grant no. RGPAS/461907. D. I. was supported by NSERC Discovery Grant no. RGPIN-2016-04314.

References

[1] Ben-Jacob, E., Cohen, I. & Levine, H. (2000) Cooperative self-organization of microorganisms. *Adv. Phys.* **49**(4), 395–554.

[2] Horstmann, D. (2004) From 1970 until present: The Keller–Segel model in chemotaxis and its consequences. II, Jahresber. *Deutsch. Math.-Verein.* **106**, 51–69.

https://doi.org/10.1017/S0956792518000013 Published online by Cambridge University Press

[3] Sherratt, J. A. (2000) Wavefront propagation in a competition equation with a new motility term modelling contact inhibition between cell populations. In: *Proceedings of the Royal Society of London A: Mathematical, Physical and Engineering Sciences*, Vol. 456, The Royal Society, pp. 2365–2386.

[4] del Castillo-Negrete, D., Carreras, B. & Lynch, V. (2002) Front propagation and segregation in a reaction–diffusion model with cross-diffusion. *Phys. D: Nonlinear Phenom.* **168**, 45–60.

[5] Ruiz-Baier, R. & Tian, C. (2013) Mathematical analysis and numerical simulation of pattern formation under cross-diffusion. *Nonlinear Anal.: Real World Appl.* **14**(1), 601–612.

[6] Tian, C., Lin, Z. & Pedersen, M. (2010) Instability induced by cross-diffusion in reaction–diffusion systems. *Nonlinear Anal.: Real World Appl.* **11**(2), 1036–1045.

[7] Gambino, G., Lombardo, M. C. & Sammartino, M. (2012) Turing instability and traveling fronts for a nonlinear reaction–diffusion system with cross-diffusion. *Math. Comp. Simul.* **82**(6), 1112–1132.

[8] Müller, J. & van Saarloos, W. (2002) Morphological instability and dynamics of fronts in bacterial growth models with nonlinear diffusion. *Phys. Rev. E* **65**(6), 061111.

[9] Rosenau, P. (2002) Reaction and concentration dependent diffusion model. *Phys. Rev. Lett.* **88**(19), 194501.

[10] Gilding, B. & Kersner, R. (2005) A fisher/kpp-type equation with density-dependent diffusion and convection: Travelling-wave solutions. *J. Phys. A: Math. Gen.* **38**(15), 3367.

[11] Kawasaki, K., Mochizuki, A., Matsushita, M., Umeda, T. & Shigesada, N. (1997) Modeling spatio-temporal patterns generated by *Bacillus subtilis*. *J. Theor. Biol.* **188**(2), 177–185.

[12] Miller, M. B., & Bassler, B. L. (2001) Quorum sensing in bacteria. *Annu. Rev. Microbiol.* **55**(1), 165–199.

[13] Liu, C., Fu, X., Liu, L., Ren, X., Chau, C. K. L., Li, S., Xiang, L., Zeng, H., Chen, G., Tang, L.-H., Lenz, P., Cui, X., Huang, W., Hwa, T. & Huang, J.-D. (2011) Sequential establishment of stripe patterns in an expanding cell population. *Science* **334**(6053), 238–241.

[14] Farrell, F., Marchetti, M., Marenduzzo, D. & Tailleur, J. (2012) Pattern formation in self-propelled particles with density-dependent motility. *Phys. Rev. Lett.* **108**(24), 248101.

[15] Tailleur, J. & Cates, M. (2008) Statistical mechanics of interacting run-and-tumble bacteria. *Phys. Rev. Lett.* **100**(21), 218103.

[16] Cates, M., Marenduzzo, D., Pagonabarraga, I. & Tailleur, J. (2010) Arrested phase separation in reproducing bacteria creates a generic route to pattern formation. *Proc. Natl. Acad. Sci. USA* **107**(26), 11715–11720.

[17] Fu, X., Tang, L.-H., Liu, C., Huang, J.-D., Hwa, T. & Lenz, P. (2012) Stripe formation in bacterial systems with density-suppressed motility. *Phys. Rev. Lett.* **108**(19), 198102.

[18] Wang, Z. & Hillen, T. (2007) Classical solutions and pattern formation for a volume filling chemotaxis model. *Chaos: An Interdiscip. J. Nonlinear Sci.* **17**(3), 037108–037108.

[19] Hillen, T. & Painter, K. (2001) Global existence for a parabolic chemotaxis model with prevention of overcrowding. *Adv. Appl. Math.* **26**(4), 280–301.

[20] Painter, K. J. & Hillen, T. (2002) Volume-filling and quorum-sensing in models for chemosensitive movement. *Can. Appl. Math. Quart.* **10**(4), 501–543.

[21] Kolokolnikov, T., Wei, J. & Alcolado, A. (2014) Basic mechanisms driving complex spike dynamics in a chemotaxis model with logistic growth. *SIAM J. Appl. Math.* **74**(5), 1375–1396.

[22] Hillen, T., Zielinski, J. & Painter, K. J. Merging-emerging systems can describe spatio-temporal patterning in a chemotaxis model. *Discrete Contin. Dyn. Syst.-Ser. B* **18**(10).

[23] Iron, D., Ward, M. & Wei, J. (2001) The stability of spike solutions to the one-dimensional Gierer–Meinhardt model. *Phys. D: Nonlinear Phenom.* **150**(1), 25–62.

[24] Doelman, A., Gardner, R. & Kaper, T. 1998 Stability analysis of singular patterns in the 1d Gray-Scott model: A matched asymptotics approach. *Phys. D: Nonlinear Phenom.* **122**(1), 1–36.

[25] Erneux, T. & Reiss, E. L. (1983) Brussellator isolas. *SIAM J. Appl. Math.* **43**(6), 1240–1246.

https://doi.org/10.1017/S0956792518000013 Published online by Cambridge University Press

[26] Kolokolnikov, T., Erneux, T. & Wei, J. (2006) Mesa-type patterns in the one-dimensional brusselator and their stability. *Phys. D: Nonlinear Phenom.* **214**(1), 63–77.
[27] Oster, G. F. & Murray, J. D. (1989) Pattern formation models and developmental constraints. *J. Exp. Zool.* **251**(2), 186–202.
[28] Maini, P., Myerscough, M., Winters, K. & Murray, J. (1991) Bifurcating spatially heterogeneous solutions in a chemotaxis model for biological pattern generation. *Bull. Math. Biol.* **53**(5), 701–719.
[29] van Kampen, N. G. (1992) *Stochastic Processes in Physics and Chemistry*. Vol. 1, Elsevier.
[30] Bressloff, P. C. (2014) *Stochastic Processes in Cell Biology*. Vol. 41, Springer, New York.

Appendix: Space-dependent Brownian motion

There is some debate in the literature as to what is the appropriate limit for the Brownian motion with spatially-dependent speed: whether it is $u_t = (s(x)u_x)_x$ or $u_t = (s(x)u)_{xx}$. In particular, the authors in [13,29] argues that any combination of these can be considered depending on the choice of methodology (Ito versus Stratonovich). For reader's convenience, here we include the derivation from first principles that argues that the correct form is $u_t = (s(x)u)_{xx}$, at least when modelling Brownian motion with space-dependent diffusion. See [30] for alternative derivation using stochastic calculus, but which gives the same result.

Consider the Brownian motion where the speed at each time step dt is chosen according to a normal distribution with a space-dependent standard deviation $\sigma = f(x)\sqrt{dt}$. The matlab code that simulates this is shown in Figure A.1.

The probability that a particle that starts at location y and time t moves to a location x at time $t + dt$ is given by $\frac{1}{\sqrt{2\pi dt f(y)}} \exp\left(-\frac{1}{2}\left(\frac{x-y}{\sqrt{dtf(y)}}\right)^2\right)$. Summing over all possible starting locations y, we obtain the following master equation:

$$u(x, d + dt) = \int_{-\infty}^{\infty} \frac{1}{\sqrt{2\pi dt f(y)}} \exp\left(-\frac{1}{2}\left(\frac{x-y}{\sqrt{dtf(y)}}\right)^2\right) u(y)dy. \tag{A.1}$$

Change variable $y = x + \sqrt{2dt}z$ so that the right-hand side becomes

$$\begin{aligned}&\int_{-\infty}^{\infty} \frac{1}{\sqrt{2\pi dt f(y)}} \exp\left(-\frac{1}{2}\left(\frac{x-y}{\sqrt{dtf(y)}}\right)^2\right) u(y)dy \\ &= \frac{1}{\sqrt{\pi}} \int_{-\infty}^{\infty} \exp\left(-z^2 \frac{1}{f^2(x+\sqrt{2dt}z)}\right) \frac{u(x+\sqrt{2dt}z)}{f(x+\sqrt{2dt}z)} dz.\end{aligned} \tag{A.2}$$

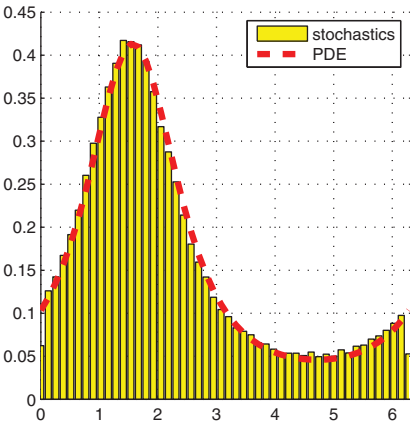
Using the standard Laplace's method, note that

$$\frac{1}{\sqrt{\pi}} \int_{-\infty}^{\infty} \exp(-z^2 h(x+\varepsilon z)) g(x+\varepsilon z) \sim g(x)h^{-1/2}(x) + \varepsilon^2 \left(\frac{g(x)h^{-3/2}(x)}{4}\right)_{xx} + O(\varepsilon^4).$$

Taking $\varepsilon = \sqrt{2dt}$, $h = 1/f^2$ and $g = u/f$ we obtain

$$\frac{1}{\sqrt{\pi}} \int_{-\infty}^{\infty} \exp\left(-z^2 \frac{1}{f^2(x+\sqrt{2dt}z)}\right) \frac{u(x+\sqrt{2dt}z)}{f(x+\sqrt{2dt}z)} dz = u(x) + \left(\left(\frac{u(x)f^2(x)}{4}\right)_{xx} dt + O((dt)^2).$$

https://doi.org/10.1017/S0956792518000013 Published online by Cambridge University Press




```
dt=0.1; N=1E5; X=zeros(1,N); a=0.5;
for sim=1:N
    x=0;
    for t=0:dt:10
        dx=randn*(1-a*sin(x))*sqrt(dt);
        x=mod(x+dx,2*pi);
    end
    X(sim)=x;
end;
clf;hold on;
[y,x]=hist(X, linspace(0,2*pi,50));
bar(x,y/N*50/2/pi,'b');
C=(1-a^2)^(3/2)/2/pi;
plot(x, C./(1-a*sin(x)).^2);
legend('stochastics', 'PDE');
```

FIGURE A.1. Left: comparison of stochastic simulation versus the PDE limit (A.3) for the Brownian motion with a space-dependent speed $f(x) = 1 - a \sin x$. Right: matlab code of the simulation that was used to produce this figure.

Taylor-expanding the left-hand side of (A.1) in dt then yields the final result,

$$u_t = \left(\frac{f^2(x)u}{4} \right)_{xx}. \tag{A.3}$$

To compare this PDE with stochastic simulations, consider the case where $f(x) = 1 - a \sin x$ with $x \in [0, 2\pi]$ with periodic boundary conditions. Then the steady-state $t \to \infty$ of (A.3) is given by $u = C/f^2 = C/(1 - a \sin x)^2$, where $C = \frac{(1-a^2)^{3/2}}{2\pi}$ is chosen so that $\int_0^{2\pi} u(x)dx = 1$. Figure A.1 shows an excellent agreement between the stochastic and its continuum limit (A.3) in this case.

https://doi.org/10.1017/S0956792518000013 Published online by Cambridge University Press